THE JOURNAL OF BIOLOGICAL CHEMISTRY
Vol. 280, No. 7, Issue of February 18, pp. 6072–6079, 2005
Printed in U.S.A.

Magnesium Regulates ADP Dissociation from Myosin V*

Received for publication, November 10, 2004, and in revised form, November 30, 2004
Published, JBC Papers in Press, December 4, 2004, DOI 10.1074/jbc.M412717200

Steven S. Rosenfeld‡§, Anne Houdusse¶, and H. Lee Sweeney‖

From the ‡Department of Neurology, University of Alabama at Birmingham, Birmingham, Alabama, 35294, ¶Structural Motility, UMR144, Institut Curie Centre National de la Recherche Scientifique, 26 Rue d'Ulm, 75248 Paris, France, and the ‖Department of Physiology, University of Pennsylvania, Philadelphia, Pennsylvania 19104

Processivity in myosin V is mediated through the mechanical strain that results when both heads bind strongly to an actin filament, and this strain regulates the timing of ADP release. However, what is not known is which steps that lead to ADP release are affected by this mechanical strain. Answering this question will require determining which of the several potential pathways myosin V takes in the process of ADP release and how actin influences the kinetics of these pathways. We have addressed this issue by examining how magnesium regulates the kinetics of ADP release from myosin V and actomyosin V. Our data support a model in which actin accelerates the release of ADP from myosin V by reducing the magnesium affinity of a myosin V-MgADP intermediate. This is likely a consequence of the structural changes that actin induces in myosin to release phosphate. This effect on magnesium affinity provides a plausible explanation for how mechanical strain can alter this actin-induced acceleration. For actomyosin V, magnesium release follows phosphate release and precedes ADP release. Increasing magnesium concentration to within the physiological range would thus slow both the ATPase activity and the velocity of movement of this motor.

A detailed understanding of chemo-mechanical transduction by the myosin family of molecular motors requires determining the structures of each of the intermediates in the myosin ATPase cycle and understanding how they are interconnected. Although a full understanding of how the myosin motor works requires knowledge of the crystallographic structures of both strong and weak actin-binding states, only the latter have been available until recently (1, 2). However, a structure of myosin V crystallized in the absence of nucleotide has now appeared, and it reveals atomic level details that are quite distinct from those of previous, weak binding structures (3). Most significant of these is a closure of the actin-binding cleft, caused by an approximation of the upper and lower 50-kDa domains. This would be predicted to enhance actin-binding affinity. Concomitantly nucleotide affinity was reduced because of a ~6.5-Å separation of the P loop from Switch I within the catalytic site. These structural features, in combination with kinetic studies on actin binding by nucleotide-free myosin V (4), have led to the suggestion that this new myosin structure represents a rigor-like conformation (3). If this is so, then it follows that between the weak binding structures previously crystallized and this new, rigor-like structure, there must also be a series of "intermediate," post-hydrolytic structures that contain within their catalytic sites ADP, magnesium, and/or phosphate. Our recent studies on the kinetics of nucleotide release from myosin V (5) are consistent with this conclusion in that they propose a series of distinct myosin-nucleotide conformations characterized by progressively higher actin affinity and progressively lower nucleotide affinity,

$$A{\cdot}(M{\cdot}D{\cdot}P_i)_{weak} \rightarrow A{\cdot}(M{\cdot}D)_{intermediate} \leftrightarrow A{\cdot}(M{\cdot}D)_{strong} \leftrightarrow A{\cdot}M_{rigor}$$

REACTION 1

where *A* is actin, *M* is myosin, and *D* is ADP. These states have been characterized by their relative actin affinities, as indicated by the subscripts "weak," "intermediate," and "strong" (5). However, another way of characterizing these states is by the contents of the catalytic site. Immediately after ATP hydrolysis, the catalytic site contains ADP, magnesium, and P_i, whereas at the end of the mechanochemical cycle, the catalytic site is empty ("rigor state"). Although phosphate is released rapidly after hydrolysis, it is not clear whether magnesium and ADP are released together or in separate steps (4, 5). If it is the latter, then each of the above states could be characterized by the contents of the catalytic site: ADP + phosphate + magnesium in one case, ADP + magnesium in the second, and ADP in the third. Recent crystallographic models of myosin V support this possibility, because they reveal a structure with ADP weakly bound and without magnesium in the catalytic site (6).

To clarify this issue, we have examined the effects of magnesium on the kinetics of ADP binding to and dissociation from actomyosin V. Our results support a model in which hydrolysis products are released in three steps, phosphate first, magnesium second, and ADP third, that are each associated with a progressively higher actin affinity. Further, they suggest that actin induces a movement of Switch I, which leads immediately to phosphate release, and that these changes in turn weaken magnesium affinity. Loss of magnesium would in turn lead to weakening of ADP affinity, followed by its dissociation. These studies also provide an explanation for how intramolecular strain could alter ADP binding to the active site, and they thereby provide a structural model for the control of processivity by this molecular motor (22–24).

EXPERIMENTAL PROCEDURES

Reagents and Proteins—The *N*-methylanthraniloyl derivative of 2′deoxy ADP was synthesized as described (7). Prepoured Sephadex G25 columns (PD10) were obtained from Amersham Biosciences. Actin was prepared from rabbit acetone powder as described (8). A myosin V S1 construct consisting of the motor domain and 1 IQ domain was prepared as described previously (4). Complexes of myosin V constructs with 2′dmD[1] were formed by preincubating S1 with a 20-fold molar excess of 2′dmD, followed by gel filtration on prepoured Sephadex G25

* This work was supported by Grants AR048565 (to S. S. R.) and AR35661 (to H. L. S.). The costs of publication of this article were defrayed in part by the payment of page charges. This article must therefore be hereby marked "*advertisement*" in accordance with 18 U.S.C. Section 1734 solely to indicate this fact.

§ To whom correspondence should be addressed: Dept. of Neurology, University of Alabama at Birmingham, FOT 1020, 1530 3rd Ave. South, Birmingham, AL 35294. E-mail: stevensr@uab.edu.

[1] The abbreviation used is: 2′dmD, 2′ deoxy mant ADP.

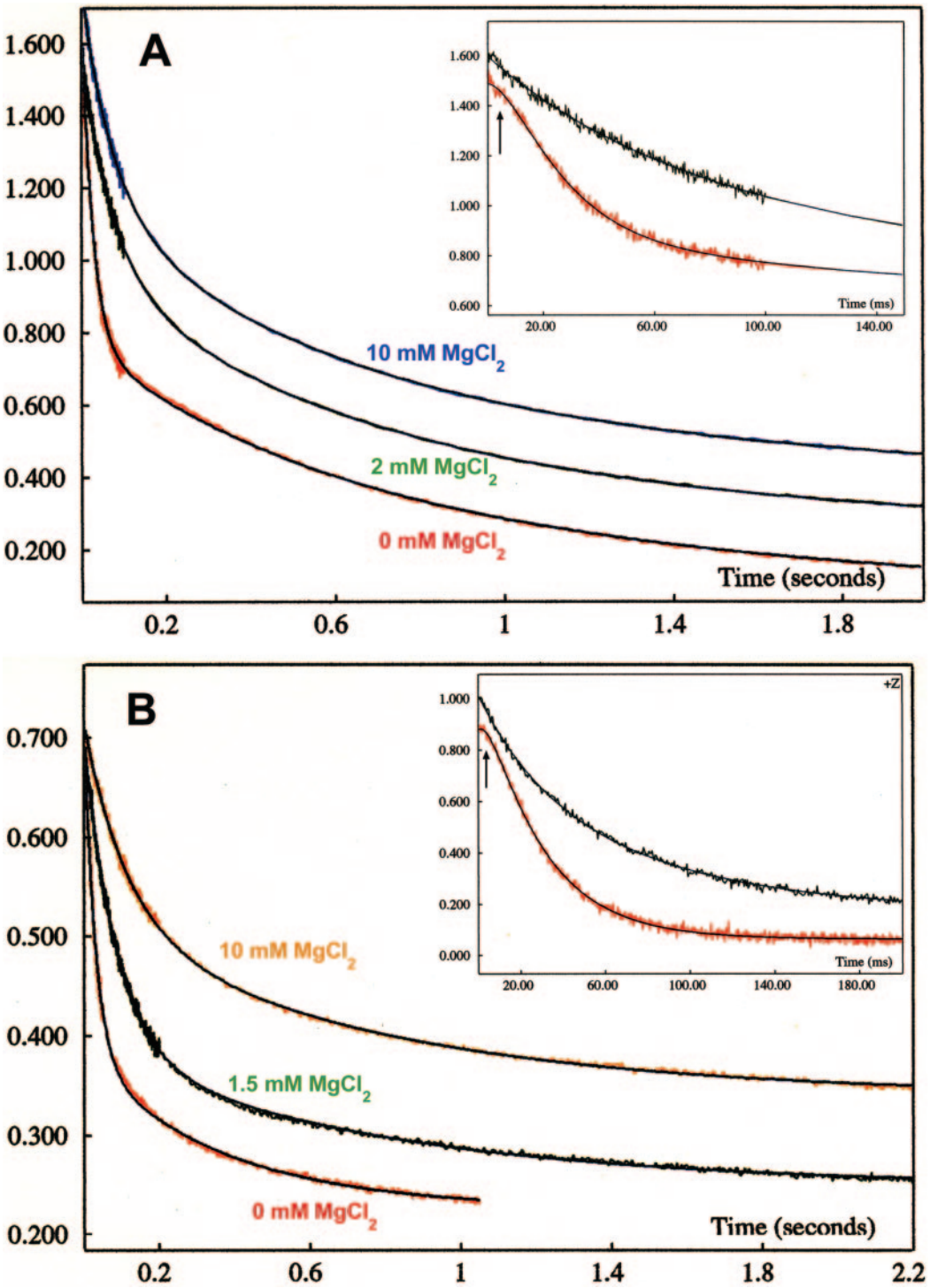

FIG. 1. **Effect of magnesium on the kinetics of 2′dmD release from myosin V (*A*) and actomyosin V (*B*).** *A*, a complex of 4 μM myosin V 1IQ·2′dmD in 75 mM KCl, 25 mM HEPES, 0.5 mM $MgCl_2$, 1 mM EGTA, 1 mM dithiothreitol, pH 7.5, was mixed in the stopped flow with 800 μM ADP in the presence of varying amounts of magnesium or in the presence of 8 mM EDTA. Release of the 2′dmD was monitored by energy transfer from vicinal tyrosine and tryptophan residues (λ_{ex} = 280 nm). Three transients are shown, for 0 mM (*red*), 2 mM (*green*), and 10 mM (*blue*) final magnesium concentration. The *jagged colored line* is the data, and the *smooth black line* is a curve fit to a three-component decay. The two faster components constituted ~90% of the total signal amplitude over all of the magnesium concentrations examined. *Inset*, a comparison of the transients at 0 mM $MgCl_2$ (*red*) *versus* 2 mM $MgCl_2$ (*green*) over a shorter time scale reveals that in the absence of magnesium, the transient is preceded by a lag (*arrow*). *B*, a complex of 4 μM myosin V 1IQ·2′dmD in 75 mM KCl, 25 mM HEPES, 0.5 mM $MgCl_2$, 1 mM EGTA, 1 mM dithiothreitol, pH 7.5, was mixed in the stopped flow with 25 μM phalloidin-stabilized actin + 800 μM ADP in the presence of varying amounts of magnesium or in the presence of 8 mM EDTA. The resulting fluorescence transients at final magnesium concentrations of 0 mM (*red*), 1.5 mM (*green*), and 10 mM (*orange*) are depicted in the figure, and they could be fit to a two-component decay (*smooth curve*) with an ~1:1 signal amplitude ratio. *Inset*, as with *A*, the transient at 0 mM $MgCl_2$ (*red*) *versus* 1.5 mM $MgCl_2$ (*green*) over a shorter time scale reveals that in the absence of magnesium, the transient is preceded by a lag (*arrow*).

columns (PD10; Amersham Biosciences) according to the manufacturer's instructions. Fractional labeling of the complexes with 2′dmD was determined by using the extinction coefficient of the fluorescent nucleotide (5700 M^{-1} cm^{-1} at 356 nm) (7) and the measured protein concentration. Ratios of 2′dmD to active site concentration were typically 0.90–0.95. Free magnesium concentrations were calculated from the

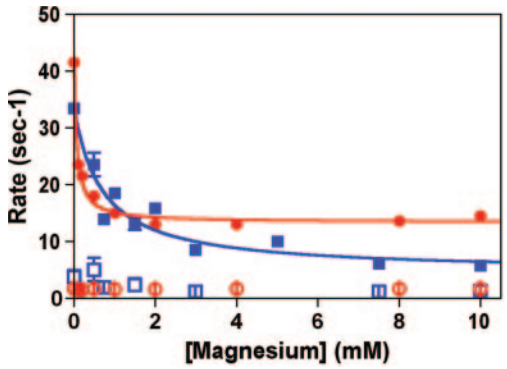

FIG. 2. **Plots of rate constants for 2′dmD release from myosin V (*red*) and actomyosin V (*blue*) *versus* magnesium concentration.** For both myosin V (*solid red circles*) and actomyosin V (*solid blue boxes*), the rate constant for the first component could be fit to Equation 1, yielding similar values of k_1 and k_1' (see Fig. 7). By contrast, actin binding increases K_a ~10-fold, from 0.07 ± 0.01 mM to 0.68 ± 0.21 mM. The rate constant for the second phase showed little magnesium concentration effect for myosin V (*open red circles*) or actomyosin V (*open blue boxes*).

stability constant for binding of magnesium to ADP (9, 10).

Kinetic Methodologies—Kinetic measurements were made at 20 °C using an Applied Photophysics SX.18MV stopped flow spectrophotometer with instrument dead time of 1.2 ms. Studies of 2′dmD binding and release were monitored by energy transfer from vicinal tryptophan residues (λ_{ex} = 280 nm), and the emission was monitored at 90° from the incident beam with a 450-nm cut-off filter (Omega Optical).

RESULTS

Effect of Magnesium on the Kinetics of ADP Release from and Binding to Myosin V—We first monitored the effects of magnesium on the kinetics of ADP release from myosin V. To do this, we mixed in the stopped flow a stoichiometric complex of 4 μM myosin V 1IQ·dmD + 0.5 mM $MgCl_2$ with 800 μM ADP in the presence of varying amounts of magnesium or in the presence of 8 mM EDTA; the latter was to generate a magnesium-free state. We calculated the final free magnesium concentration in each case, using the stability constant for binding of magnesium to the unprotonated form of ADP (9, 10). Furthermore, because the kinetics of equilibration of this reaction is extremely rapid (11, 12), particularly relative to the dead time of the stopped flow (1.3 ms), we assumed that the final concentrations of magnesium were formed by the end of the mixing phase. The dissociation of 2′dmD from myosin V was monitored by energy transfer from vicinal tryptophan and tyrosine residues, as reported in our earlier studies (5).

Fig. 1*A* illustrates examples of the resulting fluorescence transients at 0 mM (*red*) and 2 mM (*green*) and 10 mM (*blue*) final magnesium concentration. Although the transients in the presence of magnesium consisted largely of two phases of roughly equal amplitude, an additional very slow component (rate constant, 0.2–0.3 s^{-1}) could also be detected, although its amplitude was consistently <10% of the total signal amplitude (data not shown), and it was not investigated further. The rate constant of the first phase varied in an inverse hyperbolic manner with magnesium concentration (Fig. 2, *solid red circles*) and could be fit to Equation 1,

$$\lambda = \frac{k'\cdot\left(\frac{[Mg^{+2}]}{K_a}\right) + k}{\left(\frac{[Mg^{+2}]}{K_a}\right) + 1} \qquad \text{(Eq. 1)}$$

where λ is the observed rate constant, k and k' are the rate constants for the fastest phase under magnesium-free and magnesium-bound conditions, respectively, and K_a is an apparent magnesium dissociation constant. Fitting the observed rate constants (Fig. 2, *solid red line*) yielded values of k = 41.5 ± 0.7 s^{-1}, k' = 13.4 ± 0.3 s^{-1}, and K_a = 0.07 ± 0.01 mM. By contrast, the second phase showed little magnesium concentration dependence and averaged 1.63 ± 0.08 s^{-1} (Fig. 2, *open red circles*). The transient produced by mixing with 8 mM EDTA (Fig. 1*A*, *inset*, *red curve*) also contained three components: an initial lag (*arrow*) that was not seen in the presence of magnesium (*green curve*) associated with a rate constant of 154 s^{-1}, a fast decreasing phase with rate constant of 33.5 ± 0.5 s^{-1}, and a slow decreasing phase with rate constant of 1.7 ± 0.3 s^{-1} that constituted ≈20% of the total signal amplitude.

A rapid decrease in 2′dmD fluorescence, whose rate constant varies with magnesium concentration, implies that immediately after mixing, the myosin V·2′dmD complex is in a rapid equilibrium between magnesium-bound and magnesium-free states. However, the presence of a second, slower phase of similar amplitude implies that there are two myosin V·ADP states and therefore that ADP can dissociate through at least two interconnected pathways (summarized in Fig. 7, *Scheme I*). The upper tier of reactions would describe the kinetics of ADP dissociation under saturating magnesium concentrations, whereas the lower tier would describe ADP dissociation in the absence of magnesium.

Because K_a is a rapid equilibrium, the apparent rate constants for 2′dmD release, $\lambda_{1,2}$, can be defined by the following relationship that we have described previously (13, 14),

$$\lambda_{1,2} = \frac{S \pm \sqrt{S^2 - 4C}}{2} \qquad \text{(Eq. 2)}$$

where $S = \bar{k}_1 + \bar{k}_{-1} + \bar{k}_2$ and $C = \bar{k}_1\cdot\bar{k}_2$ and where

$$\bar{k}_1 = \frac{k_1'\cdot\left(\frac{[Mg^{+2}]}{K_a}\right) + k_1}{\left(\frac{[Mg^{+2}]}{K_a}\right) + 1} \qquad \text{(Eq. 3)}$$

$$\bar{k}_{-1} = \frac{k_{-1}'\cdot\left(\frac{[Mg^{+2}]}{K_b}\right) + k_{-1}}{\left(\frac{[Mg^{+2}]}{K_b}\right) + 1} \qquad \text{(Eq. 4)}$$

$$\bar{k}_2 = \frac{k_2'\cdot\left(\frac{[Mg^{+2}]}{K_b}\right) + k_2}{\left(\frac{[Mg^{+2}]}{K_b}\right) + 1} \qquad \text{(Eq. 5)}$$

Solving for the rate constants in *Scheme I* of Fig. 7 can be simplified by considering the limiting cases: no magnesium (*e.g.* in the presence of EDTA) and saturating magnesium (*e.g.* $[Mg^{2+}] \gg K_a$). However, the experiment depicted in Fig. 1*A* does not provide an independent measure of k_2 or k_2', the dissociation rate constants in the absence and presence of magnesium, respectively. To measure these values, we performed the following experiment. Nucleotide-free myosin V was mixed in the stopped flow with varying concentrations of 2′dmD in the presence of 8 mM EDTA or in the presence of 0.25, 0.5, 1, 2, and 5 mM $MgCl_2$ (final concentrations). The resulting fluorescence increase consisted of two well separated phases under all conditions (Fig. 3*A*). In the absence of magnesium, the slower phase constituted 8% of the total signal amplitude. This value increased to 29% at 5.0 mM $MgCl_2$ (data not shown). The rate constant of the faster phase varied linearly with [2′dmD], and the slopes and y intercepts, defining the apparent second order rate constant and dissociation rate constant, respectively, decreased with increasing magnesium concentration (Fig. 3*A*, *inset*). The apparent second order rate constant of the faster phase varied with magnesium concentration (Fig. 4,

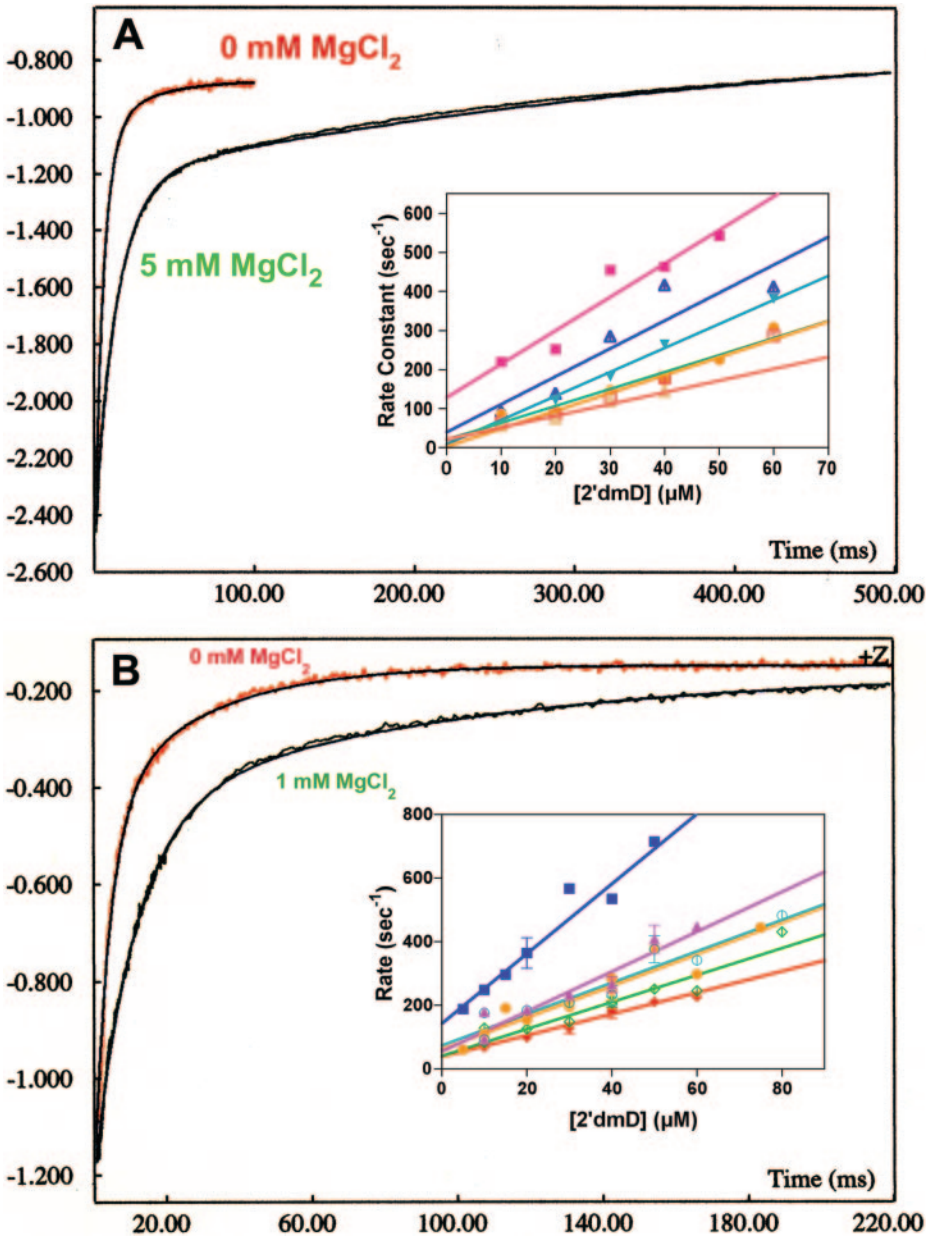

FIG. 3. **Effect of magnesium on the kinetics of 2′dmD binding to myosin V (*A*) and actomyosin V (*B*).** *A*, 4 μM nucleotide-free myosin V was mixed in the stopped flow with 40 μM 2′dmD in the presence of 8 mM EDTA (*red*) or 5 mM $MgCl_2$ (*green*). The resulting fluorescence increase consisted of two phases that could be fit to a double exponential process (*smooth curve*). *Inset*, a plot of rate constant *versus* final [2′dmD] was linear at 0 mM (*magenta*), 0.25 mM (*blue*), 0.5 mM (*green*), 1 mM (*emerald*), 2 mM (*orange*), and 5 mM (*red*) final magnesium concentrations. The slope of each plot defines an apparent second order rate constant, k_{app}, and the *y* intercept defines a dissociation rate constant. *B*, corresponding experiment with 4 μM nucleotide-free myosin V + 30 μM actin. The resulting transient consisted of two phases. *Inset*, a plot of rate constant *versus* final [2′dmD] was linear at 0 mM (*blue*), 0.5 mM (*magenta*), 1 mM (*emerald*), 2 mM (*orange*), 5 mM (*green*), and 10 mM (*red*) final magnesium concentration.

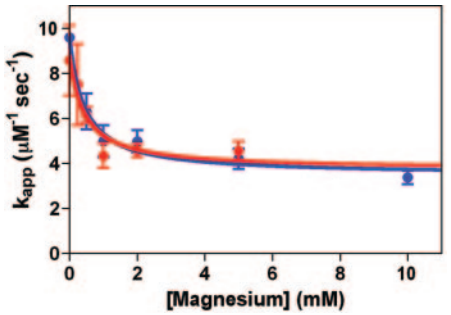

FIG. 4. **Plot of k_{app} *versus* [magnesium] for myosin V (*red*) and actomyosin V (*blue*).** For both preparations, data could be fit to Equation 1, defining values of k_{app} for magnesium-free and magnesium saturated conditions. For myosin V, k_{app} is 8.7 ± 0.9 μM^{-1} s^{-1} in the absence of magnesium, 3.7 ± 1.0 μM^{-1} s^{-1} extrapolated to infinite magnesium, and K_c = 0.6 ± 0.5 mM. For actomyosin V, the corresponding values are 9.6 ± 0.7 μM^{-1} s^{-1}, 3.5 ± 0.5 μM^{-1} s^{-1}, and 0.68 ± 0.21 mM.

red circles) in a manner described by Equation 1, yielding values of k_{-2}, k_{-2}', and K_c of 8.7 ± 0.9 μM^{-1} s^{-1}, 3.7 ± 1.0 μM^{-1} s^{-1}, and 0.6 ± 0.5 mM, respectively (Fig. 4, *red curve*). Extrapolation of the rate constant for the faster phase to the origin provides a measure of the dissociation rate constant $\bar{k}_2$. This likewise varied with magnesium concentration (Fig. 5, *red circles*), defining dissociation rate constants k_2, k_2', and K_b of 163 ± 20 s^{-1}, 15 ± 12 s^{-1}, and 0.05 ± 0.05 mM, respectively. The rate constant of the slower phase in the absence of magnesium provides a measure of $k_1 + k_{-1}$, whereas at saturating magnesium concentrations it measures $k_1' + k_{-1}'$. Note that the high apparent affinity of magnesium significantly limits the accuracy of K_b. This issue was addressed by examining the effect of magnesium on the slower phase. The rate constant for this process varied in an inverse hyperbolic manner with magnesium concentration (Fig. 6, *red circles*), defining $k_1 + k_{-1}$ = 52.2 ± 2.2 s^{-1} and $k_1' + k_{-1}'$ = 2.8 ± 1.9 s^{-1}. The magnesium concentration dependence of these rate constants provides a separate and more accurate measure of K_b of 0.12 ± 0.02 mM.

The experimentally derived values of k_2, k_2', $k_1 + k_{-1}$, and $k_1' + k_{-1}'$ allow us to solve the rate constants in *Scheme I*, and this solution is depicted in Fig. 7. The rate-limiting step in this pathway is an isomerization between two myosin V·MgADP states. This is consistent with our prior studies of other high

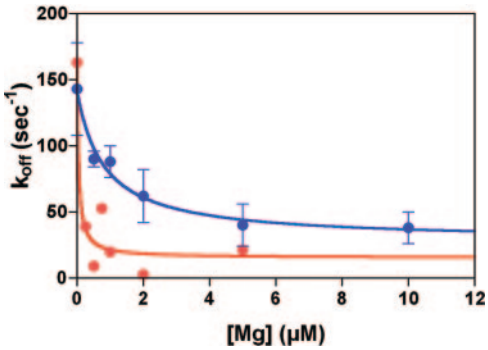

FIG. 5. **Plot of k_2 *versus* [magnesium] for myosin V (*red*) and actomyosin V (*blue*).** The data were fit to Equation 1, defining values of k_2, k_2', and K_b of 163 ± 20 s^{-1}, 15 ± 12 s^{-1}, and 0.06 ± 0.05 mM, respectively, for myosin V. The corresponding values for actomyosin V are 141 ± 16 s^{-1}, 28 ± 17 s^{-1}, and 0.81 ± 0.44 mM.

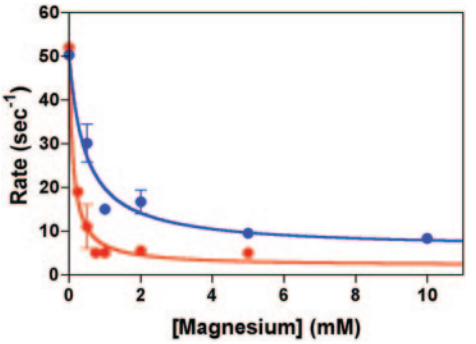

FIG. 6. **Plot of the rate constant of the slower phase in Fig. 3 *versus* [magnesium] for myosin V (*red*) and actomyosin V (*blue*).** The observed rate constant is a measure of $\bar{k}_1 + \bar{k}_{-1}$. Fitting to Equation 1 for the data with myosin V provides values of $k_1 + k_{-1}$ of 52.2 ± 2.2 s^{-1}, $k_1' + k_{-1}'$ of 2.8 ± 1.9 s^{-1}. The magnesium concentration dependence of these rate constants provides a separate and more accurate measure of K_b of 0.12 ± 0.02 mM. The corresponding values for actomyosin V are: $k_1 + k_{-1}$ = 50.6 ± 2.3 s^{-1}, $k_1' + k_{-1}'$ = 5.9 ± 2.1 s^{-1}, and K_b = 0.50 ± 0.27 mM.

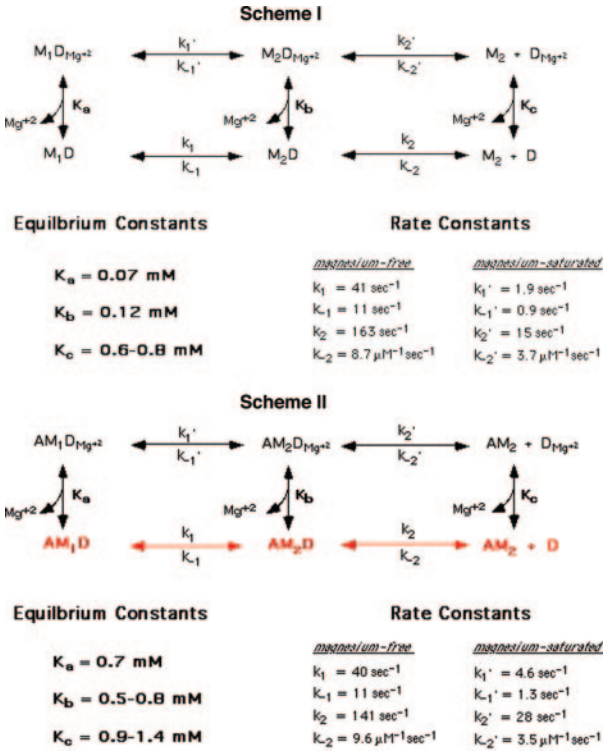

FIG. 7. **Kinetic model of magnesium regulation of ADP release from myosin V (*Scheme I*) and actomyosin V (*Scheme II*).** ADP release occurs after two sequential conformational changes in both the absence and the presence of magnesium, indicated by the subscripts 1 and 2. Rate constants under magnesium-saturated conditions are listed in the *upper tier*, and those in the absence of magnesium are in the *lower tier*. The values of K_a and K_b were determined by fitting to Equation 1, whereas K_c was derived from the values of the other equilibrium constants. Note that the major effect of actin is to markedly increase the values of K_a and K_b. This means that under physiologic conditions, magnesium is released *before* ADP dissociates from actomyosin V. Hence, the *lower tier* of reactions in *Scheme II*, highlighted in *red*, is the physiologically relevant pathway for ADP release.

duty cycle myosins, including myosin IIB (15).

Effect of Magnesium on the Kinetics of ADP Release from and Binding to Actomyosin V—Having used the results with myosin V to develop an overall kinetic scheme, we next turned our attention to actomyosin V to examine how actin affects the kinetics of ADP release. We monitored the kinetics of ADP release by mixing a complex of 2 μM myosin V 1IQ·dmD + 0.5 mM $MgCl_2$ with 20 μM actin + 800 μM ADP in the presence of varying amounts of magnesium, as was done in experiments in the absence of actin. Fig. 1*B* illustrates the resulting fluorescence transients at 0 mM (*red*), 1.5 mM (*green*), and 10 mM (*orange*) final magnesium concentration. At all of the magnesium concentrations examined, the transient could be fit to a double exponential decay (Fig. 1*B*, *solid black lines*). The rate constant of the faster phase varied with magnesium concentration in a manner that could be described by Equation 1, with k = 33.6 ± 2.1 s^{-1}, k' = 4.6 ± 2.2 s^{-1}, and K_a = 0.7 ± 0.2 mM (Fig. 2, *solid blue boxes*). The slower phase, constituting ~20–30% of the total signal amplitude, was characterized by a rate constant that showed little magnesium concentration dependence and averaged 2.7 ± 1.8 s^{-1} (Fig. 2, *open blue boxes*). As with myosin V alone, the transient for actomyosin V in the absence of magnesium also contained an initial lag (Fig. 1*B*, *inset*, *arrow*) not seen in the presence of magnesium (Fig. 1*B*, *inset*, *green transient*). The lag phase was associated with a rate constant of 145 ± 56 s^{-1}.

Finally, we examined the kinetics of binding of 2′dmD to a complex of actomyosin V by mixing nucleotide-free actomyosin V with varying concentrations of 2′dmD in the presence of 0, 0.5, 1, 2, 5, and 10 mM $MgCl_2$. As in the case of myosin V, the resulting fluorescence increase consisted of two well separated phases under all conditions (Fig. 3*B*). In the absence of magnesium, the slower phase constituted 18% of the total signal amplitude, whereas at 10 mM $MgCl_2$ it increased to 31% (*data not shown*). The rate constant of the faster phase varied linearly with [2′dmD], and the slopes and y intercepts decreased with increasing magnesium concentration (Fig. 3*B*, *inset*). The apparent second order rate constant of the faster phase varied with magnesium concentration (Fig. 4, *solid blue boxes*) in a manner described by Equation 1, yielding values of k_{-2}, k_{-2}', and K_c of 9.6 ± 0.7 μM^{-1} s^{-1}, 3.5 ± 0.5 μM^{-1} s^{-1}, and 0.68 ± 0.21 mM, respectively. The value of $\bar{k}_2$ also varied with magnesium concentration, as in the case of myosin V (Fig. 5, *solid blue boxes*), defining values of k_2, k_2', and K_b of 141 ± 16 s^{-1}, 28 ± 17 s^{-1}, and 0.81 ± 0.44 mM, respectively. Finally, the rate constant of the slower phase in Fig. 3*B* also varied with magnesium concentration, defining values of $k_1 + k_{-1}$ = 50.6 ± 2.3 s^{-1} and $k_1' + k_{-1}'$ = 5.9 ± 2.1 s^{-1} (Fig. 6, *solid blue boxes*). The magnesium concentration dependence of these rate constants provides an independent measure of K_b of 0.50 ± 0.27 mM.

Solving the rate equations with these parameters provides values of the rate constants for the case of actomyosin V. These are depicted as *Scheme II* in Fig. 7. Although there are multiple points in the pathways outlined in Scheme II where actin could exert its effect in accelerating ADP release, it is striking that the most prominent effect of actin is on the affinity of magne-

sium for the M_1·D and M_2·D states, which are reduced ~10-fold.

DISCUSSION

A Model of Magnesium-regulated ADP Release—The results of this study demonstrate that magnesium affects the dissociation kinetics of ADP from myosin V. Understanding the physiologic relevance of this finding, however, requires a detailed kinetic model that describes how magnesium affects the pathway leading to ADP dissociation. Our data support a model in which myosin V·ADP undergoes two conformational changes before nucleotide is released, indicated by the subscripts 1 and 2 in Fig. 7. Because each of these states can bind magnesium, this situation could generate multiple pathways for ADP release. Which one of these is used by myosin V under physiologic conditions? Answering this question requires determining the values of the rate and equilibrium constants in this system. We propose that after ATP hydrolysis and phosphate release, myosin V·ADP enters a rapid equilibrium described by the following,

$$\begin{array}{c} M_1{\cdot}D_{Mg^{+2}} \\ \updownarrow\ K_a \\ M_1{\cdot}D \end{array} \qquad \text{(Eq. 6)}$$

where K_a is defined by the fit to Equation 1 (0.07 mM). Transition to the M_2 state could occur either in the presence or in the absence of magnesium. The probability that magnesium would be released first, followed by formation of the M_2 state, can be determined by the following relationship.

$$\text{probability} = \frac{\bar{k}_1}{\bar{k}_1 + \bar{k}_1'} \qquad \text{(Eq. 7)}$$

At a magnesium concentration of 2.0 mM, this would be ≈45%. Thus, both the upper and lower pathways illustrated in *Scheme I* would be utilized under physiologic conditions.

Given that the K_a and K_b equilibria are rapid, Equation 2 predicts that the fluorescent decrease associated with release of 2′dmD from myosin V should be biphasic. In the presence of magnesium, adequate fitting of the data in Fig. 1*A* required three exponential terms, although the amplitude of the third term was typically <10% of the total signal amplitude. This suggests that although myosin V·ADP is mostly an equilibrium mixture of two states, there is a small fraction of an additional state.

By contrast, actomyosin V represents a very different situation. Because actin binding markedly weakens K_a and K_b, the probability that magnesium would be released prior to ADP would be 96% at 2 mM magnesium. Hence, the dominant pathway would be as follows.

$$\begin{array}{l} \mathrm{A{\cdot}M_1{\cdot}D_{Mg^{+2}}} \\ \updownarrow\ \mathrm{K_a} \\ \mathrm{A{\cdot}M_1{\cdot}D} \xrightleftharpoons{k_1/k_{-1}} A \cdot M_2 \cdot D \end{array} \qquad \text{(Eq. 8)}$$

The next step, formation of the AM_2·ADP state, is linked to ADP dissociation, which is irreversible under physiologic conditions. Given that $k_2 \gg k_2'$, this means that the predominant physiologic pathway would be,

$$\begin{array}{l} A{\cdot}M_1{\cdot}D_{Mg^{+2}} \\ \updownarrow\ K_a \\ A{\cdot}M_1{\cdot}D \xrightleftharpoons{k_1/k_{-1}} A{\cdot}M_2{\cdot}D \xrightleftharpoons{k_1/k_{-2}} A{\cdot}M_2 + D \end{array} \qquad \text{(Eq. 9)}$$

and this pathway is highlighted in *red* in *Scheme II* of Fig. 7. Mixing myosin V·2′dmD or actomyosin V·2′dmD with EDTA produced transients that contained an initial lag phase (Fig. 1, *A* and *B*, *insets*) with rate constants consistent with what would be predicted from Equation 2. However, a slower phase with a rate constant of ≈1.7 s^{-1} in the absence of magnesium would not have been predicted from either scheme in Fig. 7. This component may represent a subset of myosin V·Mg-2′dmD molecules in which the magnesium is only slowly exchangeable and in which nucleotide release only occurs along the upper pathway of *Scheme I* even in the presence of EDTA. Further studies will be necessary to determine the nature of this state and its physiologic significance.

Four conclusions are apparent from *Scheme I*. First, our finding that K_a and K_b are similar in value to each other implies that the conformational changes that underlie the M_1·D ↔ M_2·D and A·M_1·D ↔ A·M_2·D transitions do not involve major rearrangements in the structures that coordinate magnesium. A second, related conclusion is that the major effect of magnesium on these transitions is *kinetic*, not *thermodynamic*. Magnesium slows the forward and reverse rate constants for this transition in both myosin V and actomyosin V by approximately 1 order of magnitude. By contrast, our finding that the equilibrium and rate constants that describe the M_2·D ↔ M_2 + D and A·M_2·D ↔ A·M_2 + D transitions *are* affected by magnesium leads to a third conclusion: the structural elements that change conformation in *these* transitions *are* involved in magnesium coordination.

Finally, we conclude that the marked reduction in Mg^{2+} affinity produced by actin binding implies that actin alters the conformation of the structural elements involved in coordinating the divalent metal. The M_1 state represents a structural state that has been seen at high resolution for a number of myosins and has been referred to as the near rigor state, the open state, and recently, the post-rigor state (6, 16). In this state the magnesium coordination depends on an element in the nucleotide pocket known as Switch I. This is illustrated in Fig. 8, which was derived from crystallographic models of myosin V (3, 6). In our earlier work, which characterized the product release steps in myosin V, we observed a change in the fluorescence signal of mant nucleotide that was associated with release of phosphate (5). We suggested that the mant fluorophor was reporting a movement of Switch I that allows phosphate release and leads to formation of the AM_1 state. Our current data also suggests that actin binding induces the movement of Switch I, because actin binding markedly reduces magnesium affinity, an effect that could be produced by disrupting the coordination of magnesium by Switch I. As we noted above, the fact that K_a and K_b are quite similar suggests that the Mg^{2+} coordination does not markedly change between the AM_1 and AM_2 states. We propose that the AM_2 state is structurally equivalent to the recently published rigor-like state of myosin V, in which Switch I is too far from the P loop to coordinate magnesium. The transition from AM_1 to AM_2 has been described kinetically for other myosins. It occurs concomitantly with an additional lever arm movement (17, 18) and provides a mechanism for strain sensitivity in these myosins.

Although the magnesium affinity does not change between the AM_1 and AM_2 states, the ADP affinity does. In the absence of actin in the post-rigor state, magnesium is coordinated by Switch I and by the β-phosphate of ADP and the P loop (directly and via water; see Fig. 8). Upon actin binding, Switch I must move away from its post-rigor position. In the case of myosin V·ADP·P_i, this movement is coupled to phosphate release and likely is necessary to create the escape route for the phosphate (19, 20). The movement would result in loss of Mg^{2+} coordination by serine 218 of Switch I, leading to a reduced affinity for

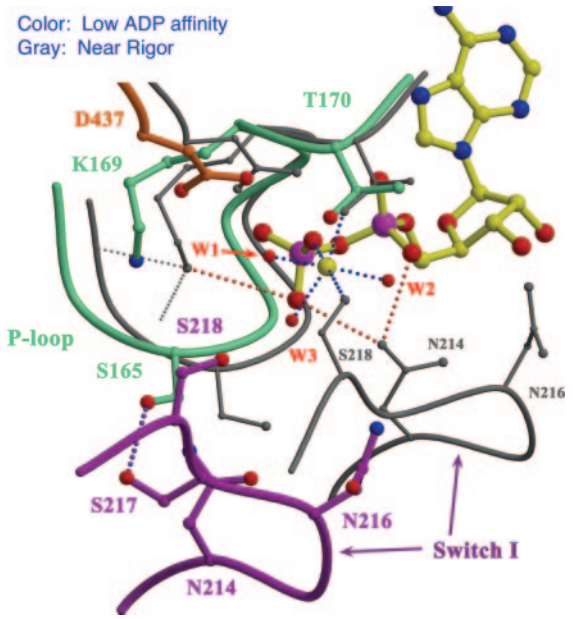

FIG. 8. **Conformational changes in the active site of myosin V.** Relative positions of the nucleotide-binding elements (P loop, *green*; Switch I, *purple*; Switch II, *orange*) that are important for ADP and Mg^{2+} coordination (*ball-and-stick*) are shown for a myosin state that binds ADP but not Mg^{2+} and is referred to as the "myosin V ADP-weak structure." The positions of the elements in the structure referred to as the "post-rigor state of myosin V" are shown in *gray* to compare the movement of these binding elements in the myosin state that strongly binds MgADP. Note in particular the Switch I and P loop movement between these two crystal structures. The *blue dotted lines* represent bonds involved in Mg^{2+} coordination in the post-rigor structure, including with three water molecules, *W1*, *W2*, and *W3*. The *red dotted lines* represent bonds involved in the coordination of the β-phosphate in the post-rigor structure, which cannot form in the ADP weak structure.

Mg^{2+}. The question is how does loss of Mg^{2+} from the AM_1 state increase the rate of isomerization from the AM_1 to the AM_2 state, leading to reduced ADP affinity. Some insights are provided by the recently published myosin V rigor-like state and a similar state with ADP (but not Mg^{2+}) bound at the active site. The nucleotide-binding elements of this ADP-bound structural state are shown in Fig. 8 and reveal that the loss of Mg^{2+} results in rearrangements of the P loop (and slight rearrangement of Switch II) as compared with the post-rigor conformation that would weaken ADP affinity (notably the loss of lysine 169). Mg^{2+} presumably would constrain these rearrangements because of the participation of threonine 170 of the P loop and aspartate 437 of Switch II (via water) in Mg^{2+} coordination. Thus, the loss of Mg^{2+} from the strong ADP-binding AM_1 state may trigger rearrangements of the P loop from its post-rigor conformation, as well as allow small rearrangements of Switch I and II. We propose that this favors the rearrangements depicted in Fig. 8. In this view, the structure in Fig. 8 (which we named the weak ADP state) is equivalent to the weak ADP-binding AM_2·ADP kinetic state defined in the current study. Concerted rearrangements of the Switch elements and P loop that follow Mg^{2+} release and that give rise to this state must be coupled to the lever arm swing associated with isomerization from the AM_1 to AM_2 states. This arrangement would confer a strain dependence. A comparison of myosin V rigor-like crystal structures with and without ADP bound reveals a further rearrangement of the P loop upon ADP dissociation (6).

A Mechanism for Strain-regulated ADP Release—Our previous study on the mechanism of myosin V processivity concluded that torsional strain on the trailing head of a myosin V dimer, which might be expected to occur as a myosin V motor steps onto a second actin filament, accelerates ADP release by ~2-fold (5). In fact, the value of the rate constant that we measured in that study is remarkably similar in value to k_1 in Fig. 7 (*Scheme II*). In light of this, we propose that strain affects the kinetics of myosin V ADP release through its effects on the release of magnesium. In our model, forward strain on the leading head would increase K_a to a value appreciably larger than the physiologic magnesium concentration of ~0.5–1.0 mM (21). In our previous study, we had shown that rearward strain blocked ADP release from the forward head (5). If rearward strain simply reduced the value of K_a, this would slow forward movement but not stop it, because ADP would be released at a rate defined by $k_1' = 4\ s^{-1}$. Rather, we propose that rearward strain must also slow the $A{\cdot}M_1 \rightarrow A{\cdot}M_2$ transition to effectively slow ADP release to the rate of MgADP release from $A{\cdot}M_1$.

Relevance to Other Myosin Isoforms—Finally, it is interesting to consider how this scheme might apply to other myosin family members. Smooth muscle myosin II, brush border myosin I, myosin VI, and nonmuscle IIB appear to use the same kinetic scheme as that used by myosin V (15, 18, 25, 26). This scheme includes a strain-dependent ADP dissociation step that is associated with an additional movement of the lever arm. However the equilibrium between those states (our $A{\cdot}M_1$ and $A{\cdot}M_2$ states) varies with temperature and with the particular isoform. For most isoforms, including smooth muscle myosin II and myosin V, it is shifted toward the $A{\cdot}M_2$ state, which would imply that magnesium release would precede ADP release. For myosin V and myosin VI, increasing magnesium concentration would be predicted to slow the steady state ATPase rate, because ADP release is rate-limiting. For all myosins, ADP release is thought to limit the maximal speed of movement, and we would predict that this in turn would be sensitive to magnesium concentration. For myosin V, this sensitivity is over the physiological range. The accompanying paper from Fujita-Becker *et al.* (27) demonstrates that myosin I displays motility that is sensitive to magnesium concentration over the physiological range. Thus, it is likely that for most myosins, the strain-sensitive isomerization that allows rapid ADP release is coupled to the release of magnesium.

REFERENCES

1. Smith, C. A., and Rayment, I. (1996) *Biochemistry* **35,** 5404–5417
2. Fisher, A. J., Smith, C. A., Thoden, J. B., Smith, R., Sutoh, K., Holden, H. M., and Rayment, I. (1995) *Biochemistry* **34,** 8960–8972
3. Coureux, P.-D., Wells, A. L., Menetrey, J., Yengo, C. M., Morris, C. A., Sweeney, H. L., and Houdusse, A. (2003) *Nature* **425,** 419–423
4. De La Cruz, E. M., Wells, A. L., Rosenfeld, S. S., Ostap, E. M., and Sweeney, H. L. (1999) *Proc. Natl. Acad. Sci. U. S. A.* **96,** 13726–13731
5. Rosenfeld, S. S., and Sweeney, H. L. (2004) *J. Biol. Chem.* **279,** 40100–40111
6. Coureux, P. D., Sweeney, H. L., and Houdusse, A. (2004) *EMBO J.* **23,** 4527–4537
7. Hiratsuka, T. (1983) *Biochim. Biophys. Acta* **742,** 496–508
8. Spudich, J. A., and Watt, S. (1971) *J. Biol. Chem.* **246,** 4866–4871
9. Smith, R. M., and Alberty, R. A. (1956) *J. Am. Chem. Soc.* **78,** 2376–2380
10. Marsh, D. J., de Bruin, S. H., and Gratzer, W. B. (1977) *Biochemistry* **16,** 1738–1742
11. Eigen, M., and Hammes, G. G. (1960) *J. Am. Chem. Soc.* **82,** 5951–5952
12. Hammes, G., and Levison, S. A. (1964) *Biochemistry* **3,** 1504–1506
13. Rosenfeld, S. S., and Taylor, E. W. (1984) *J. Biol. Chem.* **259,** 11908–11919
14. Rosenfeld, S. S., and Taylor, E. W. (1987) *J. Biol. Chem.* **262,** 9994–9999
15. Rosenfeld, S. S., Xing, J., Chen, L.-Q., and Sweeney, H. L. (2003) *J. Biol. Chem.* **278,** 27449–27455
16. Geeves, M. A., and Holmes, K. C. (1999) *Annu. Rev. Biochem.* **68,** 687–728
17. Whittaker, M., Wilson-Kubalek, E. M., Smith, J. E., Faust, L., Milligan, R. A., and Sweeney, H. L. (1995) *Nature* **378,** 748–751
18. Rosenfeld, S. S., Xing, J., Whitaker, M., Cheung, H. C., Brown, F., Wells, A., Milligan, R. A., and Sweeney, H. L. (2000) *J. Biol. Chem.* **275,** 25418–25426
19. Houdusse, A., and Sweeney, H. L. (2001) *Curr. Opin. Struct. Biol.* **11,** 182–194
20. Sweeney, H. L., Rosenfeld, S. S., Brown, F., Faust, L., Smith, J., Xing, J., Stein, L. A., and Sellers, J. R. (1998) *J. Biol. Chem.*, **273,** 6262–6270
21. Kushmerick, M. J., Dillon, P. F., Meyer, R. A., Brown, T. R., Krisanda, J., and Sweeney, H. L. (1986) *J. Biol. Chem.* **261,** 14420–14429

22. Forkey, J. N., Quinlan, M. E., Shaw, M. A., Corrie, J. E., and Goldman, Y. E. (2003) *Nature* **422,** 399–404
23. Yildiz, A., Forkey, J. N., McKinney, S. A., Ha, T., Goldman, Y. E., and Selvin, P. R. (2003) *Science*, **300,** 2061–2065
24. Mehta, A. D., Rock, R. S., Rief, M., Spudich, J. A., Mooseker, M. S., and Cheney, R. E. (1999) *Nature* **400,** 590–593
25. De La Cruz, E., Ostap, E. M., and Sweeney, H. L. (2001) *J. Biol. Chem.* **276,** 32373–32381
26. Jontes, J. D., Milligan, R. A., Pollard, T. D., and Ostap E. M. (1997) *Proc. Natl. Acad. Sci. U. S. A.* **94,** 14332–14337
27. Fujita-Becker, S., Durrwant, U., Erent, M., Clark, R. J., Geeves, M. A., and Manstein, D. J. (2005) *J. Biol. Chem.* 280, 6064–6071